Exploration of the exotic structure in Ce isotopes by the relativistic point-coupling model combined with complex momentum representation

Xue-Neng Cao,[1] Ke-Meng Ding,[1] Min Shi,[2] Quan Liu ●,[1] and Jian-You Guo ●[1,*]

[1]*School of Physics and Materials Science, Anhui University, Hefei 230601, China*
[2]*School of Mathematics and Physics, Anhui Jianzhu University, Hefei 230601, China*

The relativistic point-coupling model is combined with the complex momentum representation with resonances considered by BCS approximation, which is called the RMFPC-CMR-BCS theory. The RMFPC-CMR-BCS theory can be used to explore exotic structures in nuclei. The resonant levels near the continuum threshold can be shown to play an important role in the formation of exotic phenomena. The Ce isotopes are taken as examples, and the energy and width are obtained for the bound states and resonant states in a clear shell structure. The occupation probabilities of valence nucleons in these orbits close to the Fermi surface are calculated, and the contributions of every orbit to the nuclear density distribution are compared. It is found that several resonant levels with low-angular momentum contribute fairly diffuse density distributions, which result in the appearance of halos and giant halos in the Ce isotopes close to the neutron drip line. $^{186-190}$Ce are suggested to be halo nuclei and $^{192-198}$Ce are suggested to be giant halo nuclei, which agrees the relativistic HFB calculations and is expected to be verified in experiment.

I. INTRODUCTION

In the past decades, the objective of nuclear physics has expanded from stable nuclei to exotic nuclei far from the stability line because of the development of unstable nuclear beam technologies. Studying properties of nuclei far from the stability line has become one of the hottest topics in nuclear physics. Related experimental research and theoretical progress can be found in the literature; see [1–6] and references therein.

Since the Fermi surface in these nuclei is close to the continuum threshold, the valence nucleons are scattered easily into the continuum. The continuum, and especially the resonances in the continuum, play a critical role in the formation of exotic phenomena, such as halos [7], giant halos [8,9], deformed halos [10,11], and quantum halos [12]. The contribution of the continuum to the giant resonance mainly comes from single-particle resonances [13,14]. Hence, it is necessary to deal reasonably with the resonant states in the continuum, especially those near the threshold.

Considering the importance of resonances in exotic phenomena, physicists have developed many methods for modeling resonances. In Ref. [11], the coupled channel method was introduced for resonances in shell model calculations, the physical mechanism of the deformed halo in ^{31}Ne was explained, and several possible neutron-halo nuclei heavier than ^{37}Mg were predicted [15]. In Ref. [16], the complex scaling method was adopted for resonances in Hartree-Fock calculations, and the exotic properties of these nuclei in the

proton drip-line region around the double magic nucleus ^{48}Ni were described satisfactorily. Moreover, the Berggren representation was presented for resonances in the Hartree-Fock formalism, and the neutron-rich nuclei $^{20-22}$O and ^{84}Ni were described well [17]. The Berggren representation was also used to explore the quasiparticle resonant states with BCS for pairings in Ref. [18]. The proper treatment of the continuous states with the Green's function method was proposed in Ref. [19], and the giant halos predicted in the neutron-rich Zr isotopes were reproduced in Skyrme-Hartree-Fock calculations [9].

The aforementioned models considering resonances have achieved success in describing exotic nuclei. To involve the contribution of resonances in the relativistic mean field (RMF), which is thought to be considerably successful in describing nuclear properties, the continuum relativistic Hartree-Bogoliubov (RHB) theory was developed [7]. The continuum RHB theory has presented a satisfactory description of halo phenomena in ^{11}Li, and an interesting prediction of giant halos in the Zr and Ca isotopes [8,20]. Furthermore, the RHB theory for deformed nuclei was established, and the deformed halo in ^{42,44}Mg was predicted, where the resonances were found to play an important role [10]. In Ref. [21], the scatter-phase shift method was proposed for resonances, and the developed RMF-rBCS formalism agrees with the description of the giant halo in Ref. [8]. The resonances were explored by analytic continuation in the coupling-constant approach, and the giant halo and deformed halo were studied in the RMF calculations [22,23]. The Green's function method was also used to solve the bound and unbound problems in the RMF framework, and neutron-rich ^{120}Sn was described satisfactorily [24].

*jianyou@ahu.edu.cn

Recently, the complex momentum representation (CMR) method has been shown to be very effective for the exploration of resonances [25]. In combination with the RMF theory, the developed RMF-CMR method has presented an excellent description of the ground state properties for ^{120}Sn [25] and the physical mechanism of deformed halo in ^{37}Mg [26]. Research on the giant halo in the Zr isotopes [27] supports the prediction in Ref. [8]. In Ref. [28], the CMR method was applied to explore resonances in ^{31}Ne, suggesting a p-wave halo, consistent with the coupling-channel calculations [11]. In Ref. [29], the resonances in the neutron-rich C isotopes were investigated systemically, and ^{19}C was shown to be a neutron halo nucleus, which agrees with experimental observations as well as other theoretical calculations. The RMF-CMR method was also used to study the neutron-rich Ca isotopes [30], and the calculated results support the prediction of halos in Ref. [20].

As there is a difficulty in dealing with the terms of meson exchange in the usual RMF theory, the RMF model with point-coupling interactions (RMFPC) [31,32] was developed in which the meson exchange is replaced by the local four-point interaction between nucleons. In the RMFPC theory, the possible physical constraints introduced by the Klein-Gordon approximation in describing the mean meson field are avoided. It is easy to study the role of naturalness in effective theories of nuclear structure-related problems [33,34]. In addition, the RMFPC theory provides more opportunities to illuminate its relationship with nonrelativistic methods [35]. In practical calculations, the most widely used nonlinear coupling parameters include PC-LA [31] and PC-F1 [32]. For the parameter set PC-LA, the pairing effects are not included in the RMFPC calculations. Although the improved RMFPC with PC-F1 considers the pairings through a standard BCS method [32], the isospin dependence of the binding energy significantly deviates from the experimental data for the isotopes or isotonic chains. In Ref. [36], a density-dependent parametrization DD-PC1 was proposed, with which the binding energy, deformation, and charge radius of deformed nuclei were well reproduced. But for the spherical nuclei, the corresponding predictions are somewhat large in comparison with experiment. The newly developed effective interaction PC-PK1 [37] has improved the isospin dependence description of binding energy along the isotopic or the isotonic chains.

Since the RMFPC with PC-PK1 holds more advantages, we have developed the RMFPC-CMR theory for exotic nuclei with resonances considered by the CMR method [38]. The single-neutron resonant states in the Sn isotopes were calculated and the results were compared with calculations by the Green's function method, showing excellent agreement. For exotic nuclei, it is necessary to consider the contributions of the continuum, especially the resonances in the continuum. Due to the improper treatment of the continuum, the traditional BCS is not thought to be reliable for nuclei near the drip line [39,40]. If one can obtain the physical resonant states rather than the nonphysical continuum, the BCS is effective. The earliest work in this respect can be seen in Ref. [41]. The resonant Hartree-Fock-BCS theory was established in Ref. [42]. Further development of the resonant Hartree-Fock-

BCS theory was provided in Ref. [16]. In Ref. [18], the Berggren representation was used to explore the quasiparticle resonance with BCS. In Ref. [21], the scattering phase shift method was combined with RMF theory, and the contributions of resonances for exotic nuclei were included by pairing with the BCS approximation. Considering that the RMFPC theory is considerably successful in describing nuclear properties and the CMR is very effective in exploring resonances, it is interesting to develop the RMFPC-CMR-BCS theory for exotic nuclei.

In recent years, the study of nuclear structure for the Ce isotopes has attracted the attention of nuclear physicists. In Ref. [43], the HFB theory with Skyrme force SLy5 was used to investigate the ground state properties of the Nd, Ce, and Sm isotopes. Based on the relativistic Hartree-Fock-Bogoliubov (HFB) method, Long *et al.* have researched systemically the ground state properties of the Ce isotopes, and presented the prediction of the neutron drip line $N = 140$ using the PKA1 interactions. Particularly, they have indicated the possible existence of halos and giant halos in the Ce isotopes near the neutron drip line. Namely, ^{186}Ce, ^{188}Ce, and ^{190}Ce are normal halo nuclei, whereas ^{192}Ce, ^{194}Ce, ^{196}Ce, and ^{198}Ce may be giant halo nuclei because more than two neutrons occupy halo orbits [5,44]. Hence, further study of exotic structures in the Ce isotopes is interesting, especially for exotic phenomena in the neutron-rich Ce isotopes with $N > 126$.

In this work, we develop the RMFPC-CMR-BCS theory and explore exotic structures in Ce isotopes using the theoretical formalism. The results show that the nuclei ^{186}Ce, ^{188}Ce, and ^{190}Ce have a d-wave halo structure, and ^{192}Ce, ^{194}Ce, ^{196}Ce, and ^{198}Ce have s- and d-wave giant halo structures, which support the predictions of halos and giant halos in Ce isotopes from the relativistic HFB calculations. In particular, the contributions of every resonant level to halos are disclosed and the physical mechanism of halo formation is clarified. The theoretical formalism is sketched in Sec. II. The numerical details and results are presented in Sec. III. A summary is given in Sec. IV.

II. FORMALISM

For the convenience in the following discussions, we briefly introduce the RMFPC-CMR-BCS formalism. The starting point of this formalism is described by the Lagrange density

$$\mathcal{L} = \mathcal{L}^{\text{free}} + \mathcal{L}^{4f} + \mathcal{L}^{\text{hot}} + \mathcal{L}^{\text{der}} + \mathcal{L}^{em}, \quad (1)$$

with

$$\mathcal{L}^{\text{free}} = \bar{\psi}(i\gamma_\mu \partial^\mu - M)\psi,$$

$$\mathcal{L}^{4f} = -\frac{1}{2}\alpha_S(\bar{\psi}\psi)(\bar{\psi}\psi) - \frac{1}{2}\alpha_V(\bar{\psi}\gamma_\mu\psi)(\bar{\psi}\gamma^\mu\psi)$$
$$- \frac{1}{2}\alpha_{TS}(\bar{\psi}\vec{\tau}\psi)(\bar{\psi}\vec{\tau}\psi) - \frac{1}{2}\alpha_{TV}(\bar{\psi}\vec{\tau}\gamma_\mu\psi)(\bar{\psi}\vec{\tau}\gamma^\mu\psi),$$

$$\mathcal{L}^{\text{hot}} = -\frac{1}{3}\beta_S(\bar{\psi}\psi)^3 - \frac{1}{4}\gamma_S(\bar{\psi}\psi)^4 - \frac{1}{4}\gamma_V[(\bar{\psi}\gamma^\mu\psi)(\bar{\psi}\gamma_\mu\psi)]^2,$$

$$\mathcal{L}^{\text{der}} = -\frac{1}{2}\delta_S \partial_\nu(\bar{\psi}\psi)\partial^\nu(\bar{\psi}\psi) - \frac{1}{2}\delta_V \partial_\nu(\bar{\psi}\gamma_\mu\psi)\partial^\nu(\bar{\psi}\gamma^\mu\psi)$$

$$-\frac{1}{2}\delta_{TS}\partial_\nu(\bar{\psi}\vec{\tau}\psi)\partial^\nu(\bar{\psi}\vec{\tau}\psi)$$

$$-\frac{1}{2}\delta_{TV}\partial_\nu(\bar{\psi}\vec{\tau}\gamma_\mu\psi)\partial^\nu(\bar{\psi}\vec{\tau}\gamma^\mu\psi),$$

$$\mathcal{L}^{em} = -\frac{1}{4}F^{\mu\nu}F_{\mu\nu} - e\frac{1-\tau_3}{2}\bar{\psi}\gamma^\mu\psi A_\mu. \tag{2}$$

The meanings of all the symbols in Eq. (1) are the same as those in the literature [37]. From the Lagrange density, one can obtain the Dirac equation for nucleons as

$$[\vec{\alpha}\cdot\vec{p} + \beta(m+S) + V]\psi = \varepsilon\psi, \tag{3}$$

where $S(\vec{r})$ and $V(\vec{r})$ are the scalar and vector potentials, respectively. The bound solutions of Eq. (3) can be obtained by conventional methods. To obtain the unbound solutions for physical resonant states, we transform Eq. (3) into momentum representation as

$$\int d\vec{k}'\langle\vec{k}|H|\vec{k}'\rangle\psi(\vec{k}') = \varepsilon\psi(\vec{k}). \tag{4}$$

Equation (4) can be solved by the separation of variables with the wave functions for spherical nuclei as

$$\psi(\vec{k}) = \begin{pmatrix} f(k)\phi_{ljm_j}(\Omega_k) \\ g(k)\phi_{\tilde{l}jm_j}(\Omega_k) \end{pmatrix}. \tag{5}$$

Then, the Dirac equation (4) becomes

$$\begin{cases} Mf(k) - kg(k) + \int k'^2 dk'V_+(k,k')f(k') = \varepsilon f(k), \\ -kf(k) - Mg(k) + \int k'^2 dk'V_-(k,k')g(k') = \varepsilon g(k), \end{cases} \tag{6}$$

with

$$V_+(k,k') = \frac{2}{\pi}\int r^2 dr[V(r) + S(r)]j_l(k'r)j_l(kr), \tag{7}$$

$$V_-(k,k') = \frac{2}{\pi}\int r^2 dr[V(r) - S(r)]j_{\tilde{l}}(k'r)j_{\tilde{l}}(kr). \tag{8}$$

By solving Eq. (6) in complex momentum space, one can obtain not only bound states but also resonant states. Based on the available bound and resonant states, the pairings are dealt with in the BCS approximation. The details can be seen in Refs. [25,27]. For the convenience of readers, several primary formulas are sketched here. In the BCS approximation, the energy gap equation with resonant states becomes

$$\sum_b \frac{\Omega_b}{\sqrt{(\varepsilon_b-\lambda)^2+\Delta^2}} + \sum_r \Omega_r \int \frac{g_r(\varepsilon)}{\sqrt{(\varepsilon-\lambda)^2+\Delta^2}}d\varepsilon = \frac{2}{G}, \tag{9}$$

and the particle number equation is

$$\sum_b \Omega_b\left[1 - \frac{\varepsilon_b - \lambda}{\sqrt{(\varepsilon_b - \lambda)^2 + \Delta^2}}\right]$$

$$+ \sum_r \Omega_r \int g_r(\varepsilon)\left[1 - \frac{\varepsilon - \lambda}{\sqrt{(\varepsilon - \lambda)^2 + \Delta^2}}\right]d\varepsilon = N, \tag{10}$$

where $\Delta(G)$ is the pairing energy gap (strength), N is the particle number, $\Omega_\sigma = j_\sigma + \frac{1}{2}$ with $\sigma = b$ for bound states
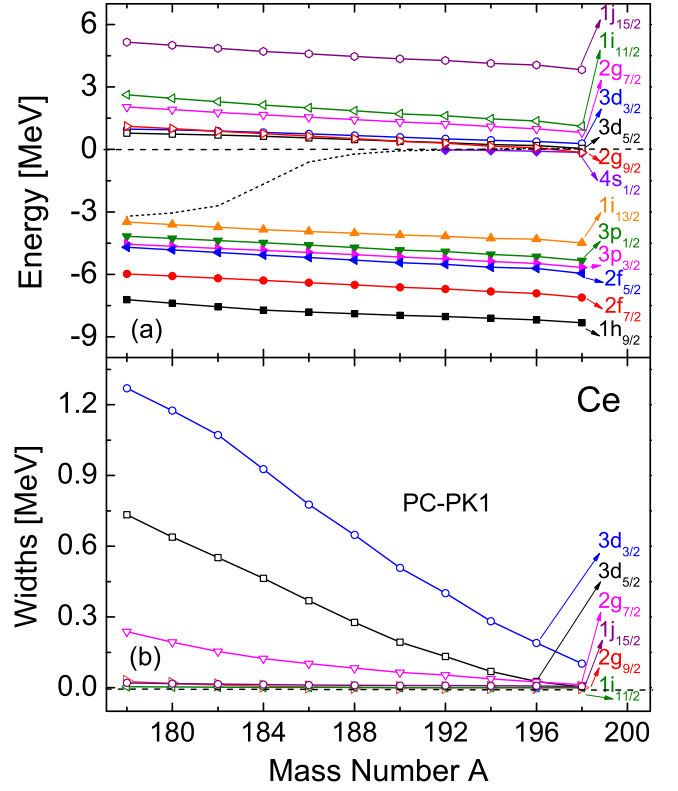

FIG. 1. The calculated neutron single-particle levels for states close to the continuum threshold in the Ce isotopes. The upper (lower) panel represents the energies (widths). These states are labeled as nl_j with n, l, and j the radial, orbital, and total angular momentum quantum numbers, respectively. The chemical potential is marked by the dashed line.

and $\sigma = r$ for resonant states, and

$$g_r(\varepsilon) = \frac{1}{\pi}\frac{\Gamma/2}{(\varepsilon - \varepsilon_r)^2 + \Gamma^2/4}, \tag{11}$$

with the real part of resonance energy ε_r and the width Γ. The solutions of Eq. (9) and (10) give us the occupation probabilities for the bound and resonant levels. With the occupations, the contributions of resonances to the density distributions and the total energy are considered naturally.

Compared with the relativistic HFB, the advantage of the present approach is that the physical mechanism of halos can be revealed from the contributions of every resonant level.

III. NUMERICAL DETAILS AND RESULTS

Based on the preceding formalism, we explore the exotic structures in the neutron-rich Ce isotopes. The numerical details are the same as those in Refs. [25,27]. An empirical formula $\Delta = 12/\sqrt{A}$ is set for the neutron and proton pairings [45]. The improved effective interactions PC-PK1 [37] is adopted in the RMFPC-CMR-BCS calculations. The available single-particle energy $E = \varepsilon_r - M$ and width Γ for these resonant states close to the continuum threshold are displayed in Figs. 1(a) and 1(b), respectively. For comparison, some bound levels near the continuum threshold are also shown

TABLE I. The calculated energies of single-particle levels near the Fermi surface in $^{178-198}$Ce in units of MeV.

Nucleus	$E(4s_{1/2})$	$E(2g_{9/2})$	$E(3d_{5/2})$	$E(3d_{3/2})$
^{178}Ce		1.11762	0.78292	0.97752
^{180}Ce		0.99944	0.7398	0.94011
^{182}Ce		0.88068	0.69188	0.88625
^{184}Ce		0.76092	0.63344	0.82182
^{186}Ce		0.64396	0.55576	0.74911
^{188}Ce		0.52401	0.47658	0.66966
^{190}Ce		0.39636	0.39627	0.58403
^{192}Ce	−0.01377	0.30368	0.3241	0.51031
^{194}Ce	−0.04387	0.1581	0.23988	0.43824
^{196}Ce	−0.08245	0.08022	0.18418	0.38306
^{198}Ce	−0.14445	−0.15871	0.05522	0.28234

in Fig. 1(a). Although the quantum numbers of these levels have been labeled on the right side of the figure, since these energy levels near the Fermi surface are very dense, we list their energies in Table I to distinguish the order of these levels, which is important for the discussion of the halo mechanism later. From Fig. 1(a) and Table I, it can be seen that there appear six resonant levels, $3d_{5/2}$, $3d_{3/2}$, $2g_{9/2}$, $2g_{7/2}$, $1i_{11/2}$, and $1j_{15/2}$, in the vicinity of the continuum threshold for the neutron-rich Ce isotopes under consideration. Without a centrifugal barrier, there does not appear the resonant level $4s_{1/2}$ in these even-even Ce isotopes with the mass numbers from $A = 178$ to $A = 190$. From the beginning of $A = 192$, there appears a weakly bound level $4s_{1/2}$. Below these resonant levels (including the weakly bound level $4s_{1/2}$) are six bound levels, $1i_{13/2}$, $3p_{1/2}$, $3p_{3/2}$, $2f_{5/2}$, $2f_{7/2}$, and $1h_{9/2}$. Between these resonant levels and bound levels, there exists a large energy gap, which favors a traditional magic number $N = 126$. If only the levels below the $N = 126$ energy gap are occupied, the halo phenomenon cannot appear. However, for the extremely neutron-rich Ce isotopes, valence neutrons may occupy these resonant levels above the $N = 126$ gap. From $A = 186$, where the Fermi surface is very close to the continuum threshold, several resonant levels are occupied, partially due to pairings. If these broad resonant levels $3d_{5/2}$ and $3d_{3/2}$ or the weakly bound level $4s_{1/2}$ are occupied partially, the nuclear density distributions become diffuse. From $A = 186$ to $A = 190$, the valence neutrons in the Ce isotopes can occupy the $3d_{5/2}$ and $3d_{3/2}$ orbits. Contrary to Ref. [44], due to a lack of a centrifugal barrier we find no resonant $4s_{1/2}$. In Ref. [44], there is a positive energy state $4s_{1/2}$, which is a canonical single-particle state, not a resonant state. From $A = 192$ to $A = 198$, there appears a weakly bound level $4s_{1/2}$. The valence neutrons in these nuclei can occupy the $4s_{1/2}$, $3d_{5/2}$, and $3d_{3/2}$ orbits, which supports the formation of a halo. Compared with Ref. [44], we have obtained exactly the resonant levels and shown the mechanism of halo formation in the Ce isotopes from $A = 186$ to $A = 198$.

In Fig. 1(b), we show the widths for the resonant levels shown in Fig. 1(a). For the broad resonances $3d_{3/2}$ and $3d_{5/2}$, their widths are considerably large. For the narrow resonances $1i_{11/2}$ and $1j_{15/2}$, their widths are very small. The widths
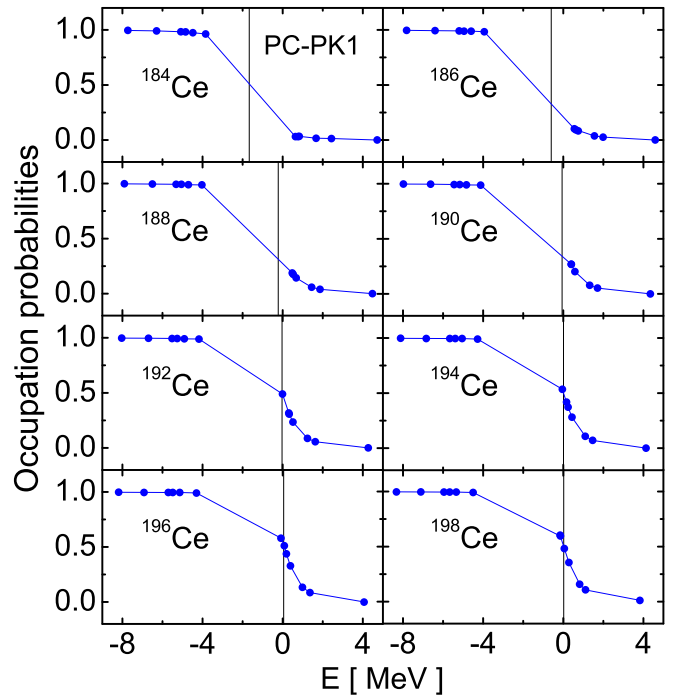

FIG. 2. The occupation probabilities v^2 in the RMFPC-CMR-BCS for Ce isotopes with mass number A as a function of the single-particle energy. The blue dots represent different energy levels, and the chemical potential is indicated by a vertical line.

for the resonances $2g_{7/2}$ and $2g_{9/2}$ lie between them. With increasing neutron number, these widths decrease monotonically. Compared with the narrow resonances, the widths for the broad resonances decline faster. Namely, the halos become more stable with increasing neutron number, especially those from the broad resonant states $3d_{3/2}$ and $3d_{5/2}$. These indicate that halos may be more easily formed in the more neutron-rich Ce nuclei.

Although these available levels support the appearance of neutron halos for the extremely neutron-rich Ce isotopes, we need to know the occupancy of the energy levels to reveal the physical mechanism of halo formation. In Fig. 2, we have presented the neutron occupation probabilities near the Fermi surface ($-9.0 < E < 5.0$ MeV) for several neutron-rich Ce isotopes. A vertical line marks the position of the chemical potential. As ^{184}Ce is a magic nucleus with neutron number $N = 126$, the orbit $1i_{13/2}$ is saturated, so we do not need to consider the contribution of the pairings for this nucleus. Starting from $N = 128$, valence neutrons will occupy these resonant levels above the $N = 126$ gap. With increasing neutron number, the occupation probabilities of these resonant levels become more and more remarkable. From $N = 128$ to $N = 132$, the valence neutrons may occupy the $3d$ and $2g$ orbits. As the $3d$ are broad resonances with lower centrifugal barrier, the occupation of these levels supports the formation of a halo. When $A \geqslant 192$, valence neutrons may occupy the $4s$, $3d$, and $2g$ orbits; the orbits $4s$ and $3d$ favor the formation of halo. With increasing mass number A, the occupation probabilities for the states $4s_{1/2}$, $3d_{3/2}$, $3d_{5/2}$ increase monotonically, which supports the existence of a possible halo structure in the neutron-rich Ce
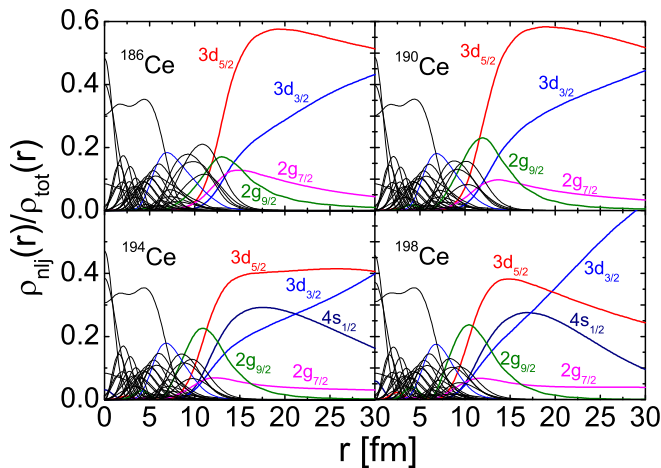
FIG. 3. The relative contributions of different orbits to the full neutron density for the PC-PK1 effective interaction in the Ce isotopes from $A = 184$ to $A = 198$. The orbits located near the particle continuum threshold are marked in different colors.
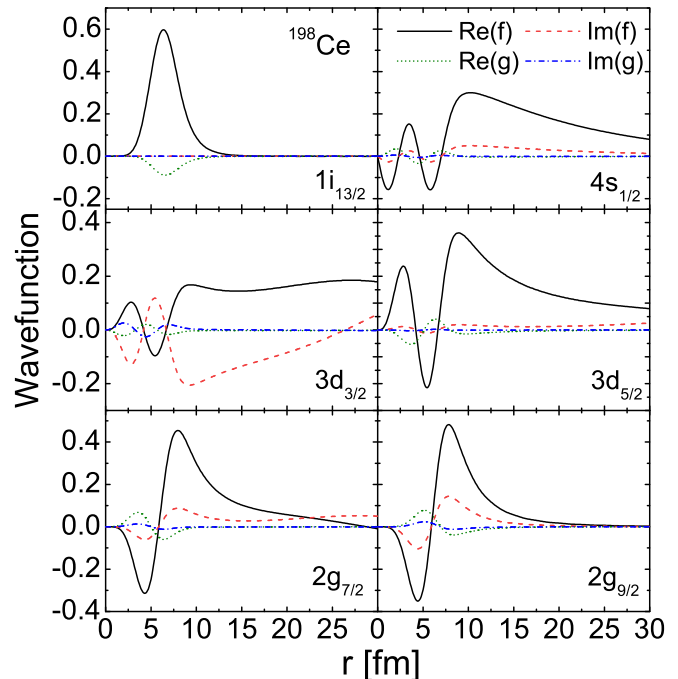

FIG. 4. Wave functions of the states $1i_{13/2}$, $4s_{1/2}$, $3d_{5/2}$, $3d_{3/2}$, $2g_{7/2}$, and $2g_{9/2}$ in ^{198}Ce. The black solid and red dashed lines represent the real and imaginary parts of the upper component $f(r)$. The olive dotted and blue dash-dotted lines represent the real and imaginary parts of the lower component $g(r)$.

isotopes. From Fig. 2, we have also observed that the particle number in the halo orbits does not exceed 2 in the nuclei ^{186}Ce, ^{188}Ce, and ^{190}Ce, which are usually called halo nuclei. For ^{192}Ce, ^{194}Ce, ^{196}Ce, and ^{198}Ce, the particle number in the halo orbits gradually increases and exceeds two particles, hence these are called giant halo nuclei. This prediction is consistent with that obtained in the relativistic HFB calculations [44].

To figure out whether these orbits can contribute a diffuse density distribution, we plot the relative contributions of different orbits to the total neutron density in Fig. 3. With the increasing radius r, the weakly bound and resonant states $4s_{1/2}$, $3d_{5/2}$, $3d_{3/2}$, $2g_{9/2}$, and $2g_{7/2}$ display diffuse density distributions, while the density distributions of the other states quickly drop to zero. As these orbits around the particle continuum threshold $4s_{1/2}$, $3d_{5/2}$, $3d_{3/2}$, $2g_{9/2}$, and $2g_{7/2}$ are gradually occupied with the increasing neutron number, the diffuse matter distributions for $^{186-190}$Ce come mainly from the contributions of the low-l states $3d_{5/2}$ and $3d_{3/2}$, and that for $^{192-198}$Ce isotopes is mostly caused by the states $4s_{1/2}$, $3d_{5/2}$, and $3d_{3/2}$. The detailed observations show that the diffuse density distributions in $^{192-198}$Ce originate mainly from the resonant levels $3d_{5/2}$ and $3d_{3/2}$. The contributions from the weakly bound level $4s_{1/2}$ to the diffuse density distributions are relatively small, which is different from Ref. [44] [see Fig. 1(b)], where the level $4s_{1/2}$ is shown to play the most important role for the halo in ^{198}Ce. Considering that the $4s_{1/2}$ is a weakly bound level, its contribution to the density distribution should decay as the radius increases. This result, the halo coming mainly from the resonant levels $3d_{5/2}$ and $3d_{3/2}$ for $^{192-198}$Ce, may be more reasonable. Due to a large centrifugal barrier, the contributions of the states $2g_{9/2}$ and $2g_{7/2}$ to the diffuse density distributions are relatively small. Nevertheless, the existence of high-l states near halo orbits is particularly important because it produces considerable energy level density around the Fermi surface and significantly enhance the pairing effect to stabilize halo isotopes.

To understand the reason why these broad resonances can contribute more disperse density distributions, in Fig. 4 we have plotted the wave functions of single-particle states for ^{198}Ce. The real and imaginary parts of the upper and lower components of the Dirac spinors are shown in Fig. 4, respectively. For the bound state $1i_{13/2}$, the upper component $f(r)$ and the lower component $g(r)$ decrease quickly to 0 with the increase of r. For the weakly bound state $4s_{1/2}$, as without the centrifugal barrier, the decay of the upper component $f(r)$ with the radius r is relatively slow. Its contribution to the dispersed density distributions is observable. Nevertheless, the wave function of the $4s_{1/2}$ decays as the radius increases since it is a bound state. Compared with the upper component $f(r)$, the contribution of the lower component $g(r)$ to the density distributions is unimportant for the level $4s_{1/2}$. For the broad resonant states $3d_{5/2}$ and $3d_{3/2}$, regardless of the real part or the imaginary part, the upper component $f(r)$ of their wave functions extends to a large range. The diffuse density distributions in ^{198}Ce come mainly from the contributions of the two resonant states. Similarly to the weakly bound state $4s_{1/2}$, the contribution of the lower component $g(r)$ to the density distributions is insignificant. For these narrow resonant states $2g_{7/2}$ and $2g_{9/2}$, the decay of the upper component $f(r)$ with the radius r is very fast because they are bound by the high centrifugal barrier. Hence, these two states do not contribute to the diffuse density distributions, although the occupation probabilities of the $2g_{9/2}$ orbit are relatively large. These indicate that the diffuse density distributions originate mainly from the broad resonant states $3d_{5/2}$ and $3d_{3/2}$.
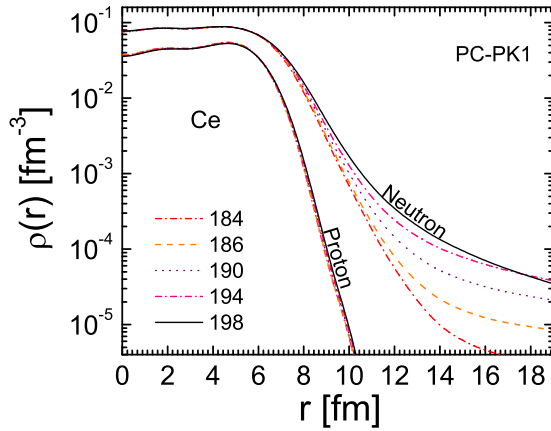
FIG. 5. The neutron density distributions of the even-even Ce isotopes from $A = 184$ to $A = 198$. For comparison, the proton density distributions are also shown.

The weakly bound state $4s_{1/2}$ also contributes to the diffuse density distributions to a certain extent. The narrow resonant and bound states almost do not contribute to the dispersion density distributions. The reason why exotic halo phenomena occur in $^{192-198}$Ce is the existence of broad resonances $3d_{5/2}$ and $3d_{3/2}$.

Since there are broad resonant states in the vicinity of the continuum threshold, it is not surprising that exotic halo phenomena may occur in the neutron-rich Ce isotopes. To make this clear, we draw the neutron density distributions in Fig. 5. For comparison, the proton density distributions are also displayed there. Although ^{184}Ce is a neutron-rich nucleus, its neutron density distributions do not show a long tail for the magic nucleus ($N = 126$). From $A = 186$ to $A = 198$, the neutron density distributions become more dispersed with the increase of mass number A. In comparison with the proton density distributions, which fall quickly with increasing radius, the neutron density distributions show a long tail, which is direct and obvious evidence of a halo. This shows that $^{186-198}$Ce are neutron halo nuclei, which we expect to be verified in experiment.

IV. SUMMARY

The relativistic point-coupling model is combined with complex momentum representation with resonances considered by BCS approximation, which is called the RMFPC-CMR-BCS theory. The RMFPC-CMR-BCS theory is used to study the ground state properties of the even-even Ce isotopes. The resonances are considered by BCS approximation with the magic nucleus ^{184}Ce as core. The available single-particle levels including the bound states and resonant states display a clear shell structure. The large gap appearing between the bound levels and resonant levels supports a traditional magic number $N = 126$ in the extremely neutron-rich Ce isotopes. The occupation probabilities of valence nucleons in these orbits close to Fermi surface are calculated, and the contributions of every orbit to nuclear density distributions are obtained. Several resonant orbits with low-angular momentum are found to contribute fairly diffuse density distributions. Compared with the contributions of different orbits to the total neutron density distribution, it is found that the diffuse density distributions in $^{186-198}$Ce come mainly from the contribution of the broad resonant states $3d_{5/2}$ and $3d_{3/2}$ although the weakly bound state $4s_{1/2}$ has also the contribution to the diffuse density distributions in $^{192-198}$Ce. This causes the total neutron density distributions to become more and more diffuse with the increase of mass number A from $A = 186$ to 198. Particularly, the occupation number in halo orbits is more than two nucleons in $^{192-198}$Ce. These suggest that $^{186-190}$Ce are halo nuclei and $^{192-198}$Ce giant halo nuclei. The calculated wave functions and neutron, proton, and matter density distributions support the conclusion. The prediction on exotic structures in the Ce isotopes is expected to be verified in experiment.

[1] I. Tanihata, H. Savajols, and R. Kanungo, Prog. Part. Nucl. Phys. **68**, 215 (2013).

[2] D. Vretenar, A. V. Afanasjev, G. A. Lalazissis, and P. Ring, Phys. Rep. **409**, 101 (2005).

[3] J. Meng, H. Toki, S. G. Zhou, S. Q. Zhang, W. H. Long, and L. S. Geng, Prog. Part. Nucl. Phys. **57**, 470 (2006).

[4] T. Niksic, D. Vretenar, and P. Ring, Prog. Part. Nucl. Phys. **66**, 519 (2011).

[5] J. Meng and S. G. Zhou, J. Phys. G: Nucl. Part. Phys. **42**, 093101 (2015).

[6] S. G. Zhou, Phys. Scr. **91**, 063008 (2016).

[7] J. Meng and P. Ring, Phys. Rev. Lett. **77**, 3963 (1996).

[8] J. Meng and P. Ring, Phys. Rev. Lett. **80**, 460 (1998).

[9] Y. Zhang, M. Matsuo, and J. Meng, Phys. Rev. C **86**, 054318 (2012).

[10] S. G. Zhou, J. Meng, P. Ring, and E. G. Zhao, Phys. Rev. C **82**, 011301(R) (2010).

[11] I. Hamamoto, Phys. Rev. C **81**, 021304(R) (2010).

[12] A. S. Jensen, K. Riisager, D. V. Fedorov, and E. Garrido, Rev. Mod. Phys. **76**, 215 (2004).

[13] P. Curutchet, T. Vertse, and R. J. Liotta, Phys. Rev. C **39**, 1020 (1989).

[14] L. G. Cao and Z. Y. Ma, Phys. Rev. C **66**, 024311 (2002).

[15] I. Hamamoto, Phys. Rev. C **95**, 044325 (2017)

[16] A. T. Kruppa, P. H. Heenen, and R. J. Liotta, Phys. Rev. C **63**, 044324 (2001).

[17] R. Id Betan, N. Sandulescu, T. Vertse, Nucl. Phys. A **771**, 93 (2006).

[18] G. G. Dussel, R. Id Betan, R. J. Liotta, T. Vertse, Nucl. Phys. A **789**, 182 (2007).

[19] E. N. Economou, *Green's Function in Quantum Physics* (Springer-Verlag, Berlin, 2006).

[20] J. Meng, H. Toki, J. Y. Zeng, S. Q. Zhang, and S. G. Zhou, Phys. Rev. C **65**, 041302(R) (2002).

[21] N. Sandulescu, L. S. Geng, H. Toki, and G. C. Hillhouse, Phys. Rev. C **68**, 054323 (2003).

[22] S. S. Zhang, X. D. Xu, and J. P. Peng, Eur. Phys. J. A **48**, 40 (2012).

[23] S. S. Zhang, M. S. Smith, Z. S. Kang, and J. Zhao, Phys. Lett. B **730**, 30 (2014).

[24] T. T. Sun, S. Q. Zhang, Y. Zhang, J. N. Hu, and J. Meng, Phys. Rev. C **90**, 054321 (2014).

[25] N. Li, M. Shi, J. Y. Guo, Z. M. Niu, and H. Z. Liang, Phys. Rev. Lett. **117**, 062502 (2016).

[26] Z. Fang, M. Shi, J. Y. Guo, Z. M. Niu, H. Z. Liang, and S. S. Zhang, Phys. Rev. C **95**, 024311 (2017).

[27] K. M. Ding, M. Shi, J. Y. Guo, Z. M. Niu, and H. Z. Liang, Phys. Rev. C **98**, 014316 (2018).

[28] Y. J. Tian, Q. Liu, T. H. Heng, and J. Y. Guo, Phys. Rev. C **95**, 064329 (2017).

[29] X. N. Cao, Q. Liu, and J. Y. Guo, J. Phys. G: Nucl. Part. Phys. **45**, 085105 (2018).

[30] M. Shi, Z. M. Niu, and H. Z. Liang, Phys. Rev. C **97**, 064301 (2018).

[31] B. A. Nikolaus, T. Hoch, and D. G. Madland, Phys. Rev. C **46**, 1757 (1992).

[32] T. Burvenich, D. G. Madland, J. A. Maruhn, and P.-G. Reinhard, Phys. Rev. C **65**, 044308 (2002).

[33] J. L. Friar, D. G. Madland, and B. W. Lynn, Phys. Rev. C **53**, 3085 (1996).

[34] A. Manohar and H. Georgi, Nucl. Phys. B **234**, 189 (1984).

[35] A. Sulaksono, T. Burvenich, J. A. Maruhn, P.-G. Reinhard, and W. Greiner, Ann. Phys. (NY) **308**, 354 (2003).

[36] T. Niksic, D. Vretenar, and P. Ring, Phys. Rev. C **78**, 034318 (2008).

[37] P. W. Zhao, Z. P. Li, J. M. Yao, and J. Meng, Phys. Rev. C **82**, 054319 (2010).

[38] Y. Wang, Z. M. Niu, M. Shi, and J. Y. Guo, Journal of Physics G **46**, 125103 (2019).

[39] J. Dobaczewski, H. Flocard, and J. Treiner, Nucl. Phys. A **422**, 103 (1984).

[40] J. Li, Z. Ma, B. Chen, and Y. Zhou, Phys. Rev. C **65**, 064305 (2002).

[41] N. Sandulescu, R. J. Liotta, and R. Wyss, Phys. Lett. B **394**, 6 (1997).

[42] N. Sandulescu, N. Van Giai, and R. J. Liotta, Phys. Rev. C **61**, 061301(R) (2000).

[43] Y. El Bassem, and M. Oulne, Int. J. Mod. Phys. E **24**, 1550073 (2015).

[44] W. H. Long, P. Ring, J. Meng, N. Van Giai, and C. A. Bertulani, Phys. Rev. C **81**, 031302(R) (2010).

[45] A. Bohr and B. R. Mottelson, *Nuclear Structure* (Benjamin, New York, 1969), Vol. I.